Supplementary information

Enhancement of CO_2 adsorption and separation in basic ionic liquid/ZIF-8 with core-shell structure

Shiyu Nie [a], Encheng Liu[b], Fengfeng Chen [a,c,*], Yilin Ma[a], Kai Chen [b,c], Junkuo Gao[a,*]

[a] Lab of Functional Porous Materials, School of Materials Science and Engineering, Zhejiang Sci-Tech University, Hangzhou 310018, China

[b] College of Textile Science and Engineering (International Institute of Silk), Zhejiang Sci-Tech University, Hangzhou 310018, China

[c] Key Laboratory of Green Cleaning Technology & Detergent of Zhejiang Province, Lishui, Zhejiang, 323000, China

[*] Corresponding author

E-mail address: cff1993@zstu.edu.cn (F. Chen), jkgao@zstu.edu.cn (J. Gao).

1. Experimental

Materials: 2-methylimidazole ($C_4H_6N_2$, 98%), zinc nitrate hexahydrate ($Zn(NO_3)_2 \cdot 6H_2O$, 98%), methanol (CH_3OH, 99%), and iminodi-acetic acid ($C_4H_7NO_4$, 98%) were purchased from Shanghai Aladdin Bio-Chem Technology Co. LTD. 1-Ethyl-3-methylimidazolium bromide (EmimBr) was purchased from the Centre of GreenChemistry and Catalysis, Lanzhou Institute of Chemical Physics, Chinese Academy of Sciences. Dowex Monosphere 550A(OH) anion exchange resin was supplied by the Dow Chemical Co. Ltd. CO_2 (99.999 wt%), N_2 (99.999 wt%), and CH_4 (99.999 wt%) were purchased from Zhejiang Jingong Energy Technology Group Co. LTD.

Synthesis of ZIF-8: The synthesis of ZIF-8 was implemented according to the previous literature.[1]

Synthesis of $[Emim]_2[IDA]$ and $[Bmim]_2[IDA]$: In a typical synthesis, an aqueous solution of 1-ethyl-3-methylimidazoliumhydroxide ([Emim][OH]) was obtained from [Emim][Br] using the anion–exchange resin method according to the previous work (Fig. S1). An iminodiacetic acid was added to the aqueous [Emim][OH] solution. Then, the mixture was stirred at 30 ℃ for 4 h. Subsequently, the mixture was transferred in a rotary evaporator to remove the water at 60 ℃. Then, the resulting liquid was dried under a vacuum at 80 ℃ for 48 h. $[Emim]_2[IDA]$ was finally obtained as the pale-yellow liquid. $[Bmim]_2[IDA]$ was synthesized by a similar method using [Bmim][OH] instead of [Emim][OH].[2]

Synthesis of the $[Emim]_2[IDA]$/ZIF-8: The $[Emim]_2[IDA]$ and ZIF-8 were dried overnight in a vacuum drying oven at 373 K before the synthesis of the composites. The $[Emim]_2[IDA]$ (120 mg) was dissolved in a methanol solution (15 mL), and the activated ZIF-8 powder (200 mg) was added to the methanol solution. Then, the methanol solution was continuously stirred under an open atmosphere at 303 K until the methanol solution was completely volatilized naturally. The obtained powder samples were dried overnight in a vacuum oven at 373 K. $[Bmim]_2[IDA]$/ZIF-8 was synthesized by a similar method using $[Bmim]_2[IDA]$ instead of $[Emim]_2[IDA]$. It is

worth noting that IL would not be lossy during the preparation process, and thus we can precisely control the loading amount of IL in ZIF-8 by adding different amounts of IL in the synthesis.

2. Characterization

Scanning electron microscopy (SEM) images of the ZIF-8 and $[Emim]_2[IDA]$/ZIF-8 were obtained using a Zeiss Evo LS 15 scanning electron microscope equipped with a Bruker XFlash 5010 Energy dispersive X-ray (EDX) detector. Transmission electron microscopy (TEM) images were obtained using FEI Talos F200S. The X-ray diffractometer (XRD) used Cu Ka radiation as the diffraction source, the wavelength was 0.1543 nm, the operating voltage was 40 kV, and the current was 40 mA. The diffraction data were collected in a two-theta range of 3-40°. The BET surface area and pore size analysis were measured by N_2 adsorption at 77 K on a Micromeritics Beishide 3H-2000PS2 instrument. Before the analyses, the samples were degassed at 80 ℃ for 4 h. The thermogravimetric analysis (TGA) was performed on a Shimadzu (TGA-50) instrument under flowing N_2 (40 mL min^{-1}) with a heating rate of 20 ℃ min^{-1}. The Fourier transform infrared (FTIR) spectra of synthesized $[Emim]_2[IDA]$ and $[Emim]_2[IDA]$/ZIF-8 were obtained using the Bruker-VERTEX 33 spectrometer. All the spectra were collected with a resolution of 4 cm^{-1} in the range of 400-4000 cm^{-1}.

3. Gas adsorption-desorption experiments

To evaluate the equilibrium separation properties of the $[Emim]_2[IDA]$/ZIF-8, the single-component gas adsorption-desorption experiments of CO_2, N_2, and CH_4 on $[Emim]_2[IDA]$/ZIF-8 and ZIF-8 were carried out on a Micromeritics physisorption analyzer (ASAP 2020 Plus) at 298 K and 100 kPa. The samples (80-200 mg) were activated overnight under a dynamic vacuum at 353 K to remove all the guest molecules before the sorption experiments were performed. The samples were activated 1 h under a dynamic vacuum at 333 K after adsorption-desorption experiments to ensure CO_2 complete desorption.

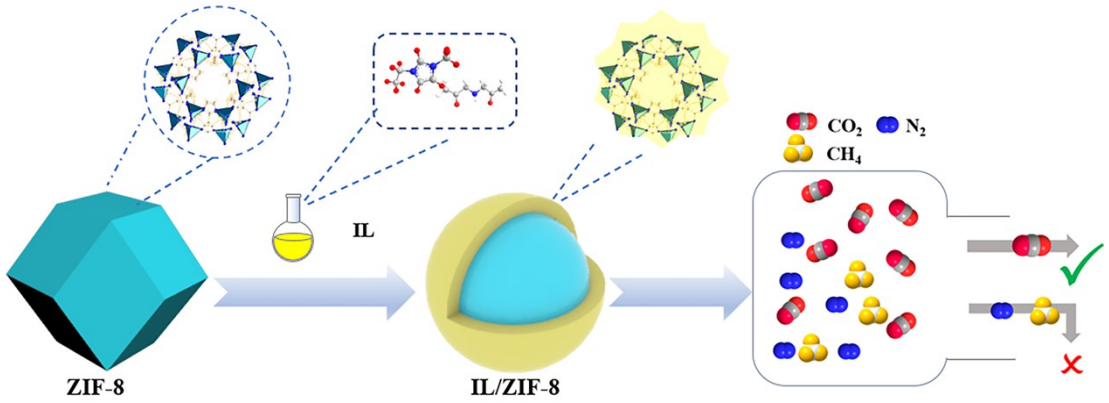

Fig. S1. A schematic representation of the synthesis and utilization of $[Emim]_2[IDA]$/ZIF-8.

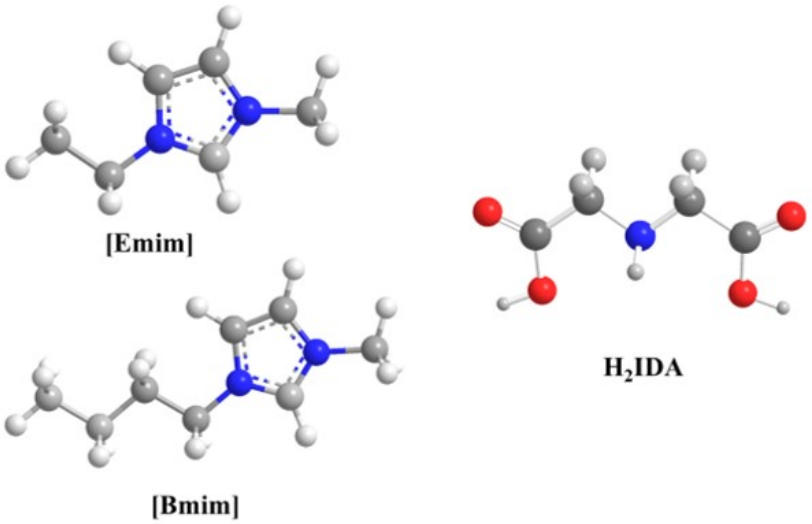

Fig. S2. The structural formula of $[Emim]_2[IDA]$ and $[Bmim]_2[IDA]$.

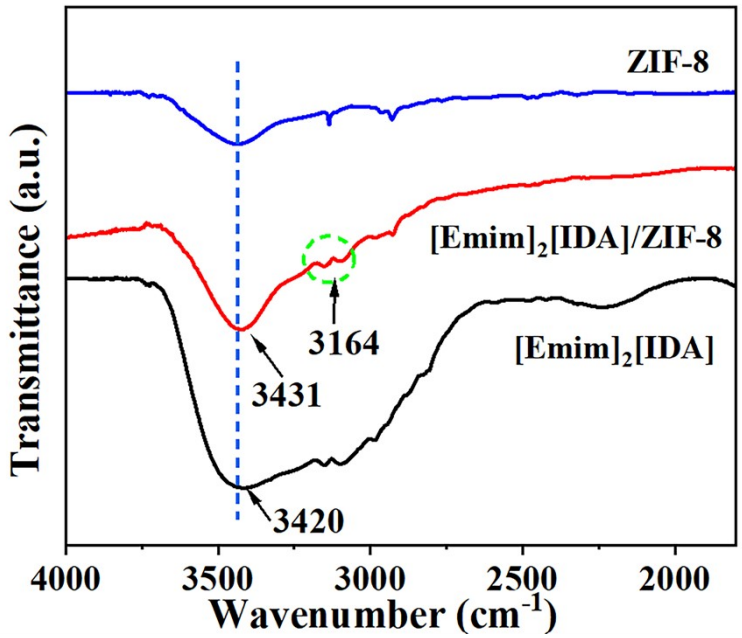

Fig. S3. FTIR spectra of ZIF-8, $[Emim]_2[IDA]$ and $[Emim]_2[IDA]$/ZIF-8 on 1700-4000 cm^{-1}.

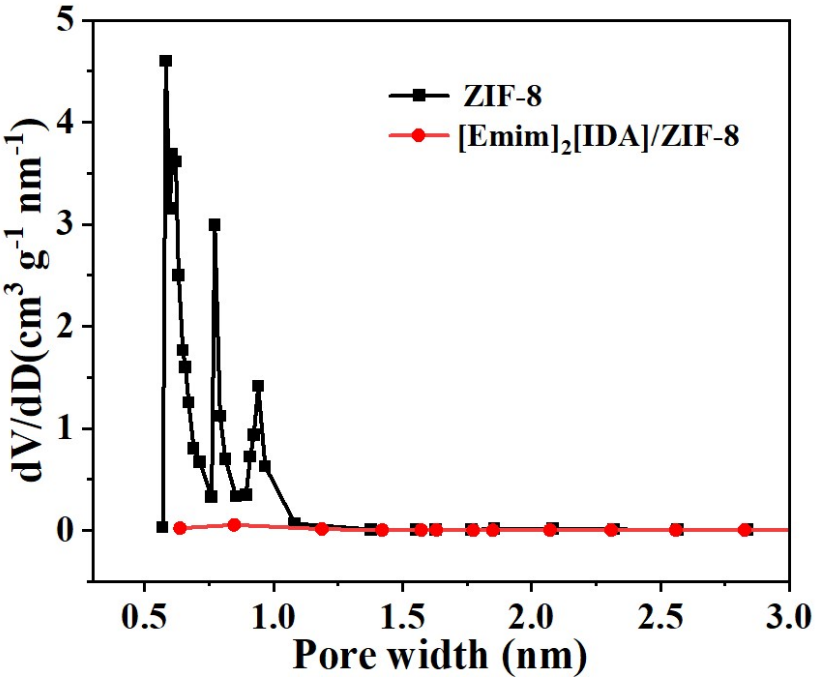

Fig. S4. pore size distribution of ZIF-8 and $[Emim]_2[IDA]$/ZIF-8.

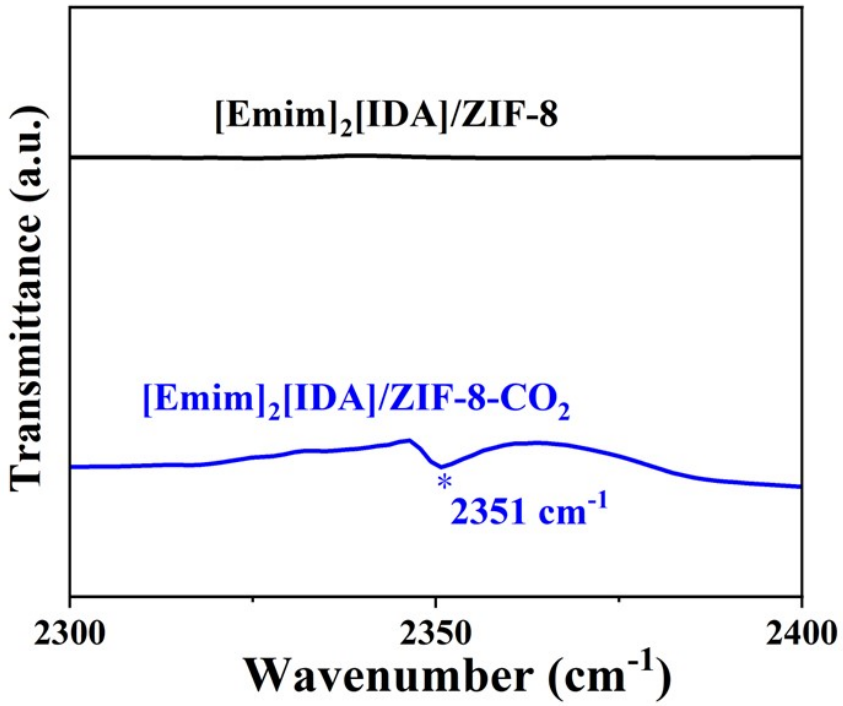

Fig S5. FTIR spectra of $[Emim]_2[IDA]/ZIF-8$ and $[Emim]_2[IDA]/ZIF-8$ after CO_2 adsorption.

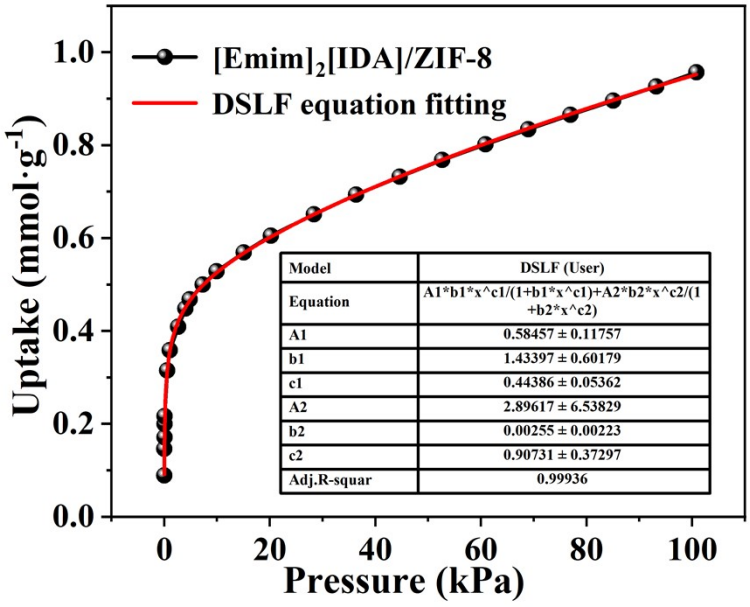

Fig. S6. The dual-site Langmuir-Freundlich equation fitting of CO_2 sorption isotherm for $[Emim]_2[IDA]/ZIF-8$.

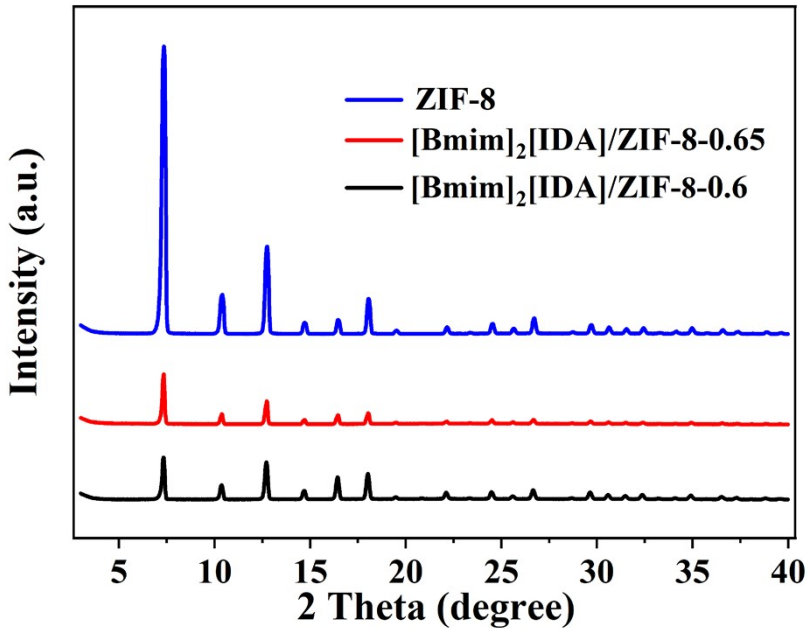

Fig. S7. XRD patterns of ZIF-8, $[Bmim]_2[IDA]$/ZIF-8-0.65, and $[Bmim]_2[IDA]$/ZIF-8-0.6.

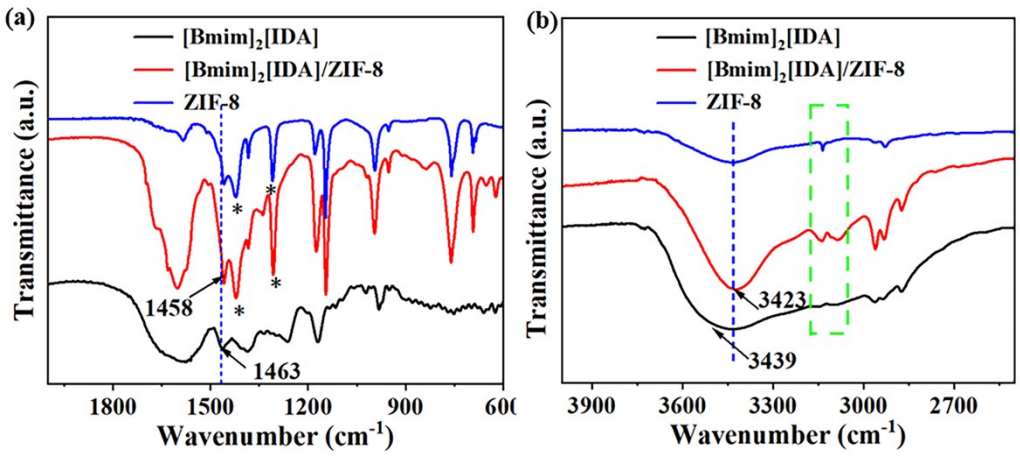

Fig. S8. FTIR spectra of ZIF-8, $[Bmim]_2[IDA]$, and $[Bmim]_2[IDA]$/ZIF-8 on (a) 600-1700 cm^{-1} and (b) 2600-3900 cm^{-1}.

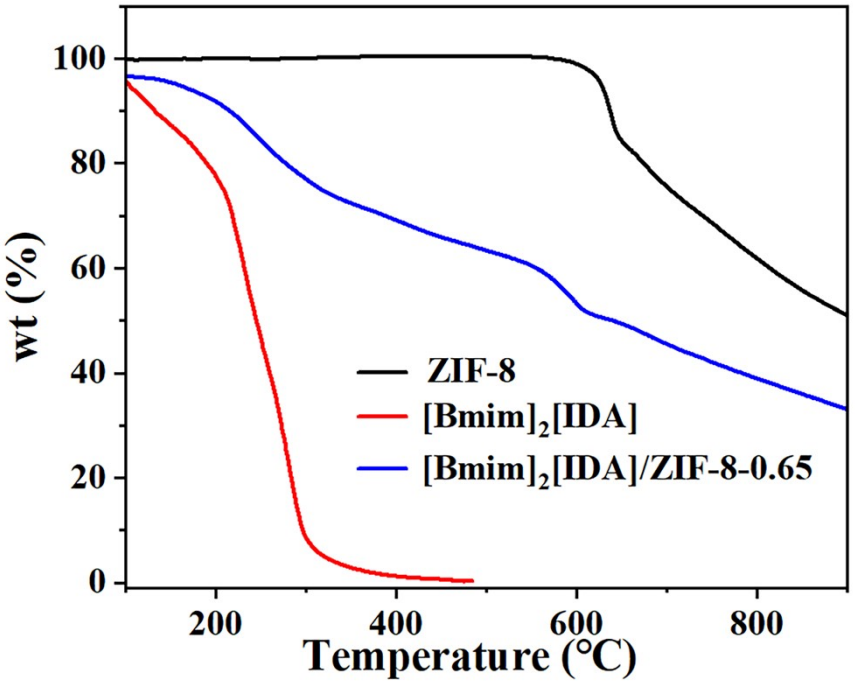

Fig. S9. TGA curves of ZIF-8, $[Bmim]_2[IDA]$, and $[Bmim]_2[IDA]$/ZIF-8-0.65.

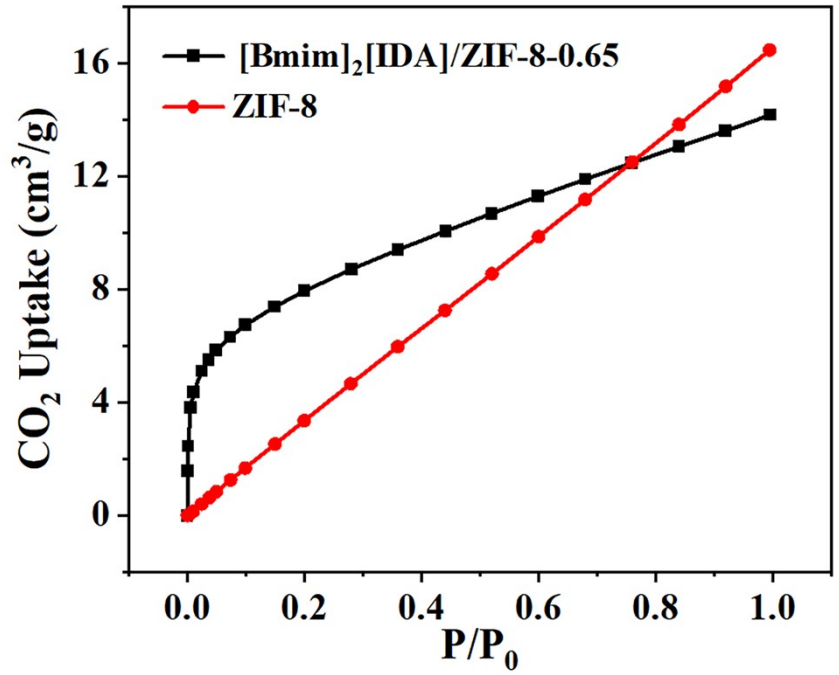

Fig. S10. CO_2 sorption isotherm for $[Bmim]_2[IDA]$/ZIF-8-0.65 at 298 K and 100 kPa.

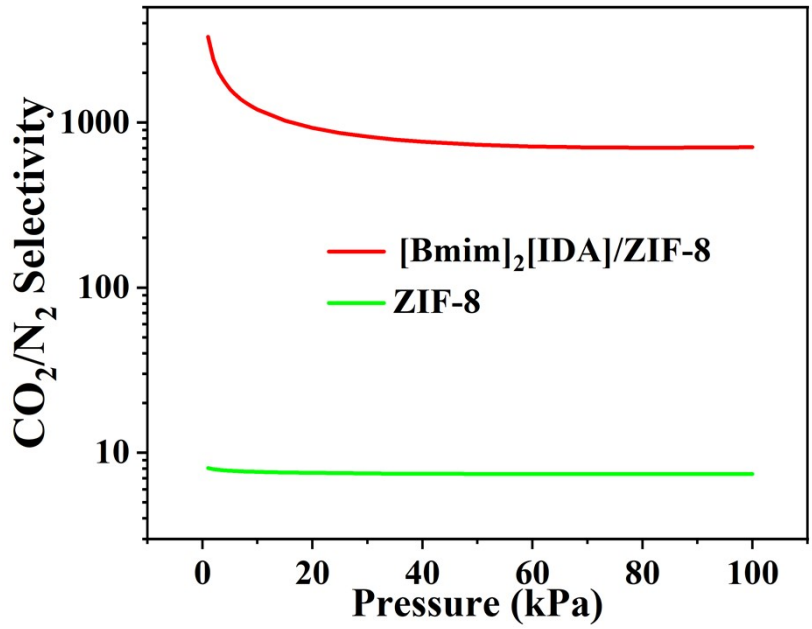

Fig. S11. The IAST-predicted adsorption selectivity for CO_2/N_2 of ZIF-8 and [Bmim]$_2$[IDA]/ZIF-8.

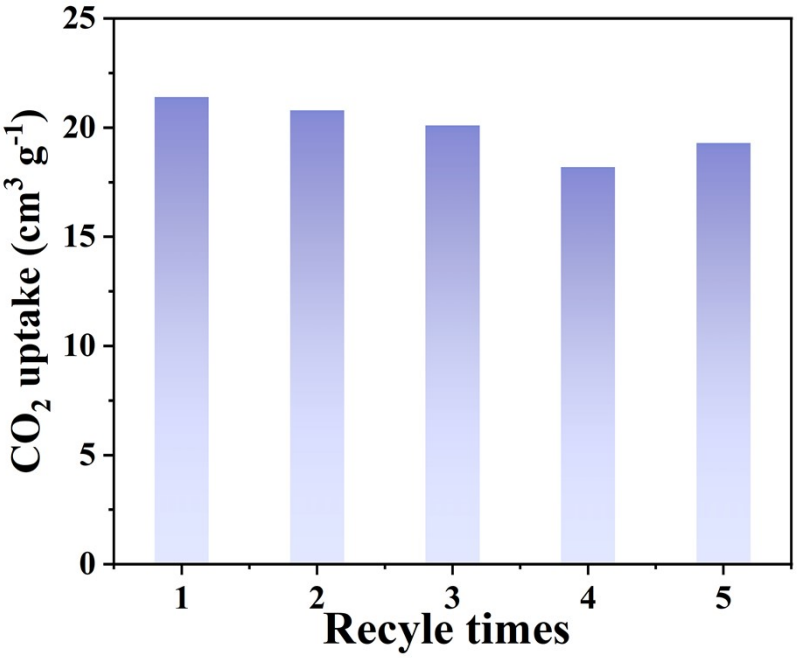

Fig. S12. Cyclic regeneration experiments for CO_2 adsorption in [Emim]$_2$[IDA]/ZIF-8 at 298 K and 100 kPa.

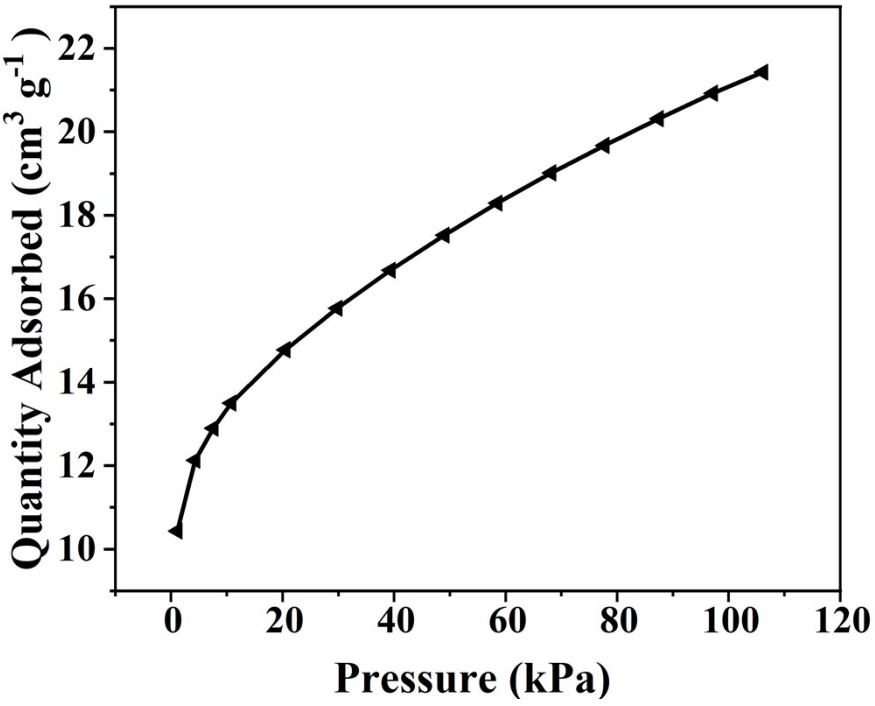

Fig S13. CO_2 desorption isotherms of $[Emim]_2[IDA]$/ZIF-8.

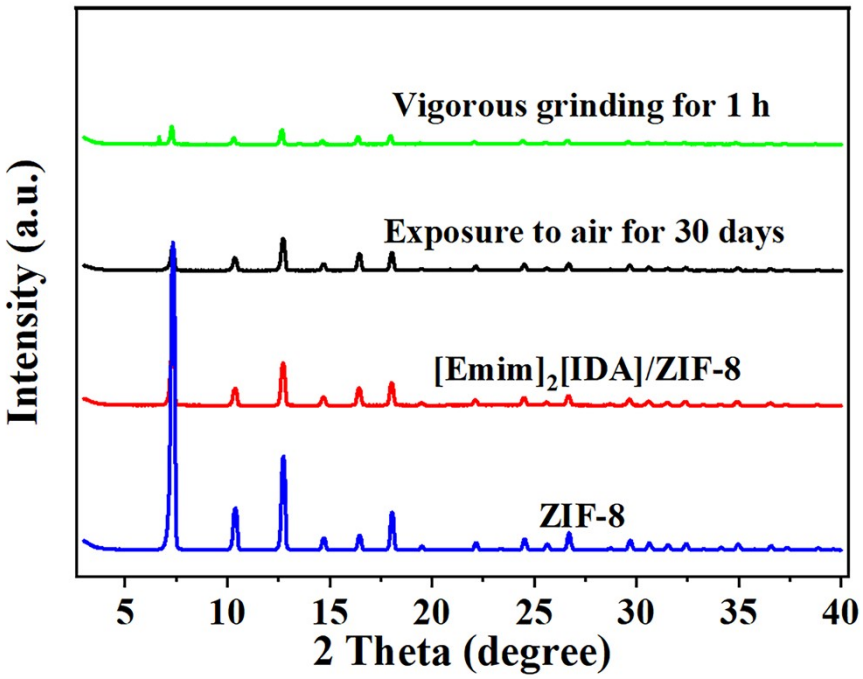

Fig. S14. PXRD patterns of ZIF-8 and $[Emim]_2[IDA]$/ZIF-8 before and after the treatment under various conditions.

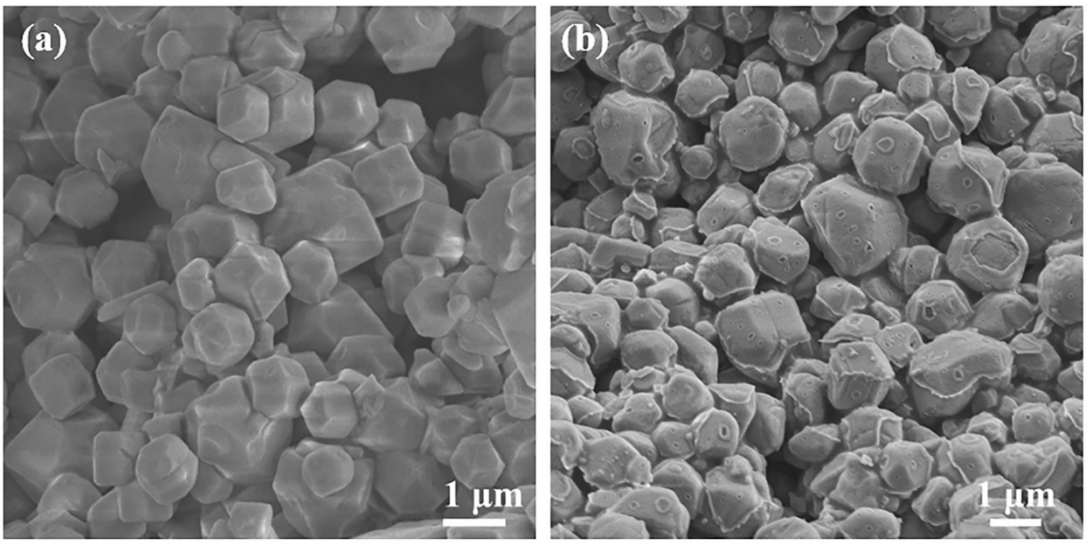

Fig. S15. SEM images of $[Emim]_2[IDA]$/ZIF-8 after (a) vigorous grinding for 1 h and (b) exposure to air for 30 days.

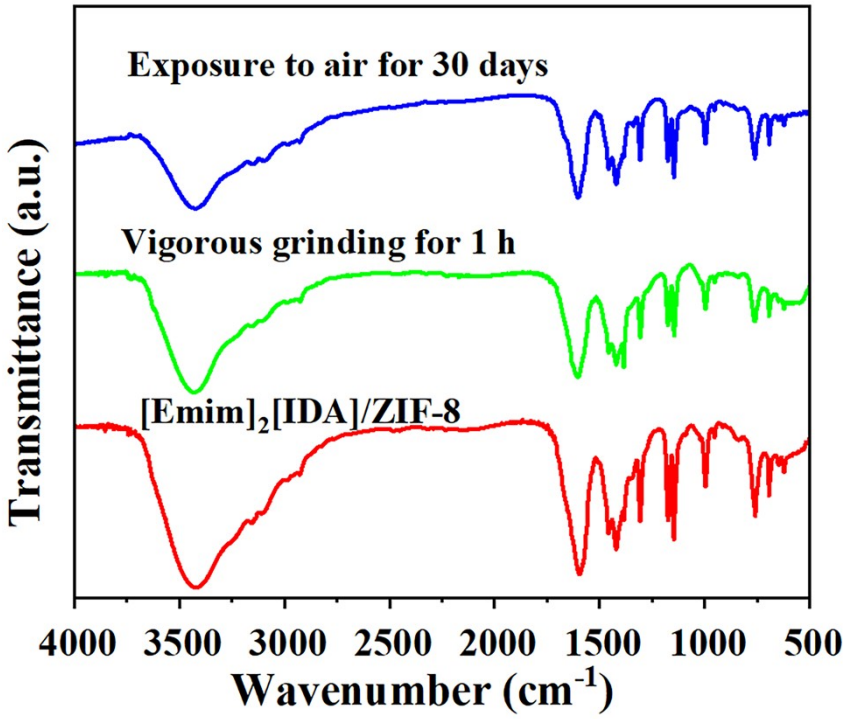

Fig. S16. FTIR spectra of $[Emim]_2[IDA]$/ZIF-8 before and after treatment under different conditions.

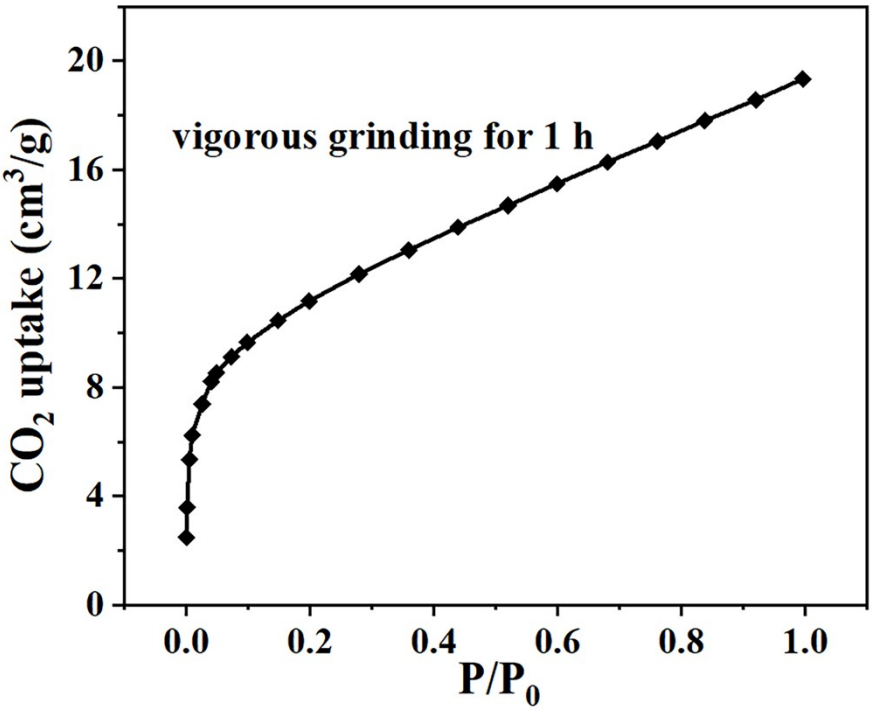

Fig. S17. CO_2 adsorption isotherms of $[Emim]_2[IDA]$/ZIF-8 after vigorous grinding for 1 h at 298 K and 100 kPa.

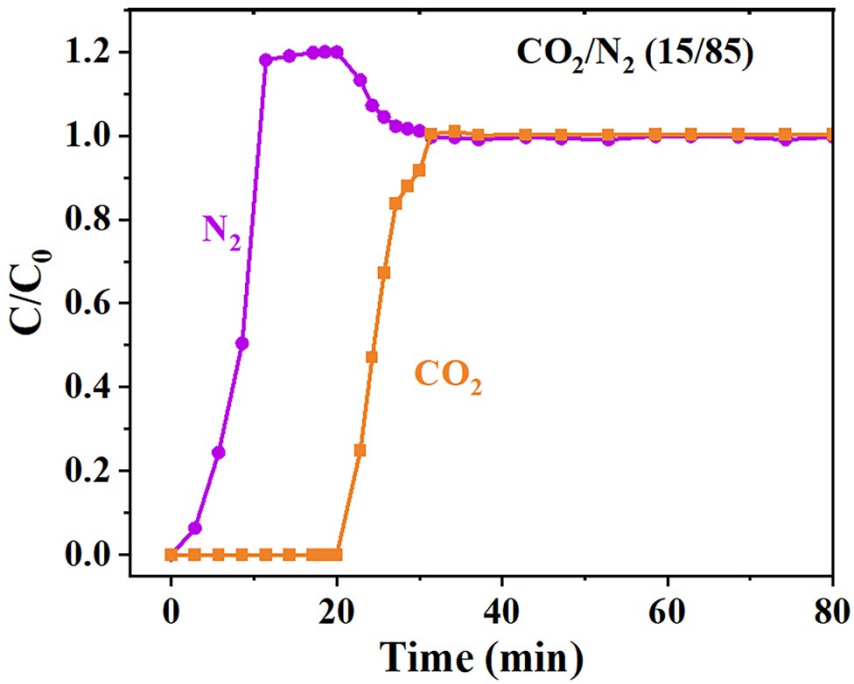

Fig. S18. Breakthrough curve of $[Emim]_2[IDA]$/ZIF-8 for CO_2/N_2 (15/85) binary gas mixture at 298 K.

Column breakthrough experiments: Column breakthrough experiments were performed using CO_2/N_2 (15/85, v/v) gas mixtures flowing over a packed column filled

with $[Emim]_2[IDA]$/ZIF-8 powder at 298 K to assess the actual separation performance of $[Emim]_2[IDA]$/ZIF-8 for CO_2/N_2 gas mixtures (Fig. S15). To our delight, a clear separation of CO_2 from CO_2/N_2 gas mixtures was achieved. Before CO_2 was discovered in the packed column's effluent, N_2 eluted first via the packed column and produced a high-purity N_2 (≥99.9%) in the outflow. As shown in Fig. S15, the breakthrough curve for CO_2/N_2 displays a distinct roll-up effect, attributed to the competitive adsorption of CO_2 and N_2. CO_2 and N_2 were simultaneously adsorbed before saturation. The breakthrough curve indicates that the N_2 gas rapidly permeates the packed column within the first minute, while CO_2 doesn't appear until 21 min. This suggests a strong interaction between the $[Emim]_2[IDA]$/ZIF-8 and CO_2 with a little adsorption of N_2. The material's low cost and high stability, combined with the positive experimental results, showcase its potential as a promising candidate for CO_2/N_2 separation. The material also yields high-purity CO_2, making it even more desirable. The utilization of low-cost raw materials, reusable solvents, and biodegradable waste, along with the implementation of straightforward operating procedures, has enabled the cost-effective and eco-friendly preparation of $[Emim]_2[IDA]$/ZIF-8. These features make it a promising candidate for practical applications.

Table S1. Distribution of elements in the EDS pattern of ZIF-8.

Element	Wire type	Wire type	Weight percentage
C	K	41.82	61.10
O	K	17.85	22.37
N	K	6.88	7.55
Zn	L	33.45	8.98
Weight		100	100

Table S2. Distribution of elements in the EDS pattern of $[Emim]_2[IDA]$/ZIF-8.

Element	Wire type	Wire type	Weight percentage
C	K	44.83	59.77
O	K	21.68	24.79
N	K	9.57	9.58
Zn	L	23.93	5.86
Weight		100	100

Table S3. Textural properties of ZIF-8, $[Emim]_2[IDA]$/ZIF-8, and $[Bmim]_2[IDA]$/ZIF-8.

Sample type	BET surface area (m^2/g)	Langmuir surface area (m^2/g)	Total pore volume (cm^3/g)	Average pore width (nm)
ZIF-8	1161.2	1729.4	0.6369	0.7989
$[Emim]_2[IDA]$/ZIF-8	60.64	89.90	0.0418	0.7506
$[Bmim]_2[IDA]$/ZIF-8	10.11	-	0.0197	-

Table S4. Comparison of the CO_2 adsorption capacity and CO_2/N_2, CO_2/N_2 selectivity of different materials from different references.

Samples	T (k)	CO_2 (cm^3 g-1)	CO_2/N_2 selectivity	CO_2/CH_4 selectivity	Ref.
ZIF-8	298	15.7	7	2.7	This work
$[Emim]_2[IDA]$/ZIF-8-0.65	298	22.45	15028	348	This work
bmimAc@ZIF-8	303	20.1	8	-	3
UiO-66	298	47	18	6	2
[Emim][Ac]@UiO-66	298	56	72	11.4	2
IL-ZIF-IL	298	34	5572	1190	4
[HEMIM][DCA]@ZIF-8	298	10.9	-	117	5
MIL-53(Al)	294	49	4.5	3	6
ZIF-68	298	1.74	19	5	7
NUT-1	298	38.9	29000	400	8
NUT-2	298	22.1	8000	360	8
NUT-3	298	14.33	1600	90	8

References

1. X. M. Ma, F. F. Chen, X. Zhang, T. T. Wang, S. R. Yuan, X. S. Wang, T. J. Li, and J. K. Gao, New J. Chem., 2022, **46**, 7528-7536.
2. S. Y. Nie, F. F. Chen, T. B. Shen, T. T. Wang, N. Y. Di and J. K. Gao, New J. Chem., 2023, **47**, 2257-2263.
3. M. Mohamedali, H. Ibrahim, A. Henni, Chem. Eng. J., 2018, **334**, 817-828.
4. G. P. Han, N. Yu, D. H. Liu, G.G. Yu, X. C. Chen and C. L. Zhong, AIChE J., 2021, **67**, e17112.
5. M. Zeeshan, V. Nozari, M.B. Yagci, T. Isik, U. Unal, V. Ortala, S. Keskin and A. Uzun, J. Am. Chem. Soc., 2018, **140**, 10113-10116.
6. P. Mishra, H. P. Uppara, B. Mandal and S. Gumma, Ind. Eng. Chem. Res., 2014, **53**, 19747-19753.
7. R. Banerjee, H. Furukawa, D. Britt, C. Knobler, M. O'Keeffe and O. M. Yaghi, J. Am. Chem. Soc., 2009, **131**, 3875-3877.
8. L. B. Sun, Y. H. Kang, Y. Q. Shi, Y. Jiang and X. Q. Liu, ACS Sustain. Chem. Eng., 2015, **3**, 3077-3085.